

Thermodynamic analysis of methane dry reforming: Effect of the catalyst particle size on carbon formation



Nicolas Abdel Karim Aramouni^{a,b}, Joseph Zeaiter^{a,*}, Witold Kwapinski^b, Mohammad N. Ahmad^a

^a Department of Chemical and Petroleum Engineering, American University of Beirut, Lebanon

^b Department of Chemical Sciences, Faculty of Science and Engineering, Bernal Institute, University of Limerick, Ireland

ARTICLE INFO

Keywords:

Dry reforming
Methane
CO₂
Syngas
Ni catalyst

ABSTRACT

The effect of catalyst particle size on thermodynamic equilibrium of methane dry reforming and carbon formation has been studied through the Gibbs free energy minimization method taking into account the deviation of carbon formed from graphite Gibbs energy and its dependence on catalyst particle size. Methane and CO₂ conversions are maximized at low pressure and high temperature, and a molar H₂/CO ratio of 1 is obtained at 1100–1200 K and 5–10 bar. Carbon formation was found to increase with particle diameter, and carbon presence was noticed at conditions of high pressure/low temperature and high temperature/low pressure. Optimal operating conditions were found to be close to carbon limits, highlighting the need for active metal particle size to be less than 5–6 nm to minimize coking. CO was identified as the precursor for carbon at low temperature, while CH₄ was found to be the main precursor at high temperature.

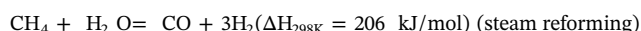
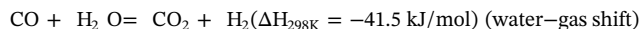
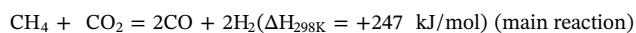
1. Introduction

The ongoing depletion of fossil fuels is driving the world to search for alternative, sustainable and renewable sources of energy [1] to meet its ever increasing energy demand [2]. Furthermore, global warming and environmental consequences from the continuously growing economies, in addition to environmental regulations, require new energy sources to produce less pollutants such as SO_x, NO_x and greenhouse gases. In parallel, the population growth has caused waste to be generated at a higher rate [3] and frequently mismanaged [4,5]. Landfill is a widely used method of municipal solid waste disposal, especially in developing countries such as Lebanon [5], and large amounts of greenhouse gases, especially carbon dioxide and methane, are produced in landfills.

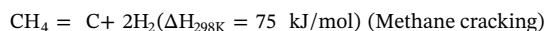
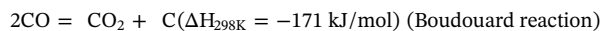
Hydrogen is a promising alternative fuel due to its high efficiency and clean combustion [6]. It is also attractive as a renewable energy source since it can be produced from biomass, water and solar energy [7]. Steam reforming has been the most common process to produce hydrogen from hydrocarbon feedstock, especially methane from natural gas, through further processing of the syngas product, essentially composed of hydrogen, carbon monoxide, CO₂ and water. Traditionally, ammonia synthesis has been the primary consumer of syngas [8]. However, more recent developments in the field of hydrocarbon reforming allowed for a better control of syngas composition, making it a very desirable feedstock for gas to liquid applications. Recently, it has

been of interest to use biogas from landfills or anaerobic digestors as a feedstock for syngas production through the dry reforming process, both due to the expected syngas H₂/CO ratio being close to unity, which is suitable for gas-to-liquid applications and Fischer-Tropsch synthesis [9,10], and due to the possibility of recycling two greenhouse gases, methane and CO₂, into useful products.

The main reactions governing the process are as follows:



In addition to the carbon formation reactions



For more comprehensive set of possible reaction see the work of Nikoo and Amin [11].

The industrial application of the dry reforming process, however, has been heavily hindered by the performance of catalysts [12–16]. Traditional, nickel-based catalysts used in reforming technologies are cheap and active, but are prone to deactivation by sintering and carbon deposition [17]. This problem is more severe in the case of dry reforming, where the endothermic nature of the reaction requires high

* Corresponding author.

E-mail address: jz08@aub.edu.lb (J. Zeaiter).

Nomenclature

G^T	total Gibbs free energy, J/mol
n_i	moles of species i
ΔG_{fi}^0	standard Gibbs energy of formation (298 K), J/mol
\bar{f}_i	partial fugacity of species i (Pa)
f_i^0	standard state fugacity of species i
R	universal gas constant, 8.314 J/mol K
P	pressure, Pa

y_i	mole fraction of i in the gas phase
μ_i	chemical potential of species i , J/mol
ΔG_c^{dev}	graphite deviation Gibbs energy, J/mol
d	particle diameter, nm
a_{ij}	moles of element i per moles of species j
b_i	initial moles of species i
T	temperature, K
Φ_i	fugacity coefficient of species i

operating temperatures. The increased presence of carbon in the feed gas as compared to steam reforming or dry reforming, in addition to the elevated temperatures, causes a significant amount of carbon to form on the catalyst, leading to quick deactivation [18]. Sintering of the nickel particles during operation leads to a loss of dispersion, ultimately leading to catalyst deactivation and increased carbon formation [19]: Carbon layers that grow from nuclei on step sites on the nickel particle are stable above 80 atoms in diameter (approximately 6 nm), meaning that larger particles are more likely to yield carbon. Noble metals, such as ruthenium or rhodium, are less prone to coking and have a high dispersion [20,21], but are very expensive and hence their use is limited.

It is imperative to model the reactions and carbon formation in order to decide on the optimal operating conditions for the reforming process. The first indication to the feasibility of the process is a thermodynamic evaluation of the equilibrium conditions to estimate the expected conversion and carbon formation. This can be done through the computation of the equilibrium constants based on standard ΔH and ΔG values [22,23], entropy maximization calculations [24] or Gibbs energy minimization routines [6,11,25–30]. The Gibbs minimization method has been widely used due to its simplicity and its ability to compute equilibrium compositions even for systems where the reaction pathways are not known. Challiwala et al. [28] noted that many studies assumed the gas phase behaved as an ideal gas, while the group's work, amongst others cited above, use non-ideal equations of state to model the non-ideal gas-phase such as the Peng-Robinson and Soave-Redlich-Kwong equations of state.

The majority of thermodynamic studies in reforming have accounted for carbon formation tendencies with the assumption that the carbon species formed is graphite, which has a zero standard Gibbs energy of formation and negligible dependence of fugacity on operating conditions, [11,28,31], with the exception of Atashi et al. [29] and Ayodele et al. [32] who have ignored carbon formation within the dry reforming process in their simulations, and Nematollahi et al. [33] who incorporated the activity of graphite into their model. However, practical experience has shown that three general types of carbonaceous species can be distinguished on a used reforming catalyst based on temperature programmed hydrogenation (TPH) studies [34]: C_α refers to surface carbide that can be hydrogenated below 323 K, C_β (or amorphous carbon) can be hydrogenated between 373 and 573 K, while C_γ (graphitic carbon) is only hydrogenated above 673 K. Electron microscopy imaging shows that filamentous carbon 'whiskers' often grow from nickel and non-noble active metal particles, and many studies have noted that carbon filaments, and carbon deposits on reforming catalysts in general, deviate from graphite thermodynamics. Whisker carbon is the most dangerous form of carbon growing on a catalyst due to its high strength. Whisker growth can cause pore damage and detachment of active metal particles from the support, leading to dusting and increased pressure drop, hot bands and eventually plant shutdown [35]. It has been observed that the Boudouard reaction and methane cracking reactions have lower equilibrium constants than graphite formation [8,36,37].

Alstrup [38] studied the formation of carbon filaments on Ni, Ni-Cu and Ni-Fe catalysts and found deviations from graphite deposition

thermodynamics that are dependent on particle size, irrespective of the (non-noble) active metal. In the same study, the author combined his finding to those of Rostrup-Nielsen [39] and proposed an expression for the deviation from the Gibbs free energy of graphite in function of the size of the largest particle catalyzing filament growth: ΔG_c^{dev} (kJ/mol) = 2.6 + 93/d (nm).

To the knowledge of the authors, such a deviation has not been considered in a thermodynamic analysis of a reforming process prior to this work. The practical implications of this deviation are twofold: On one hand, there is some uncertainty around the present carbon limits calculated in thermodynamic studies. On the other hand, the carbon limits in a reformer are a function of the catalyst particle size: in other terms, the age of the bed, and consequently the severity of sintering in the catalyst batch, affects the carbon limits and it is then possible to define dynamic carbon limits from a semi-empirical approach. By incorporating the deviation parameter, this study shows the impact of non-graphite behavior and bed aging on the main parameters of the dry reforming process. The intricate reaction mechanism on the catalyst surface, in addition to the added complexity of modeling carbon whisker formation on a catalyst particle makes it very difficult to use a set of chemical reactions as a basis for thermodynamic equilibrium [40]. The Gibbs energy minimization method was chosen to model the chemical equilibrium of the process while incorporating the deviation Gibbs energy into the model while avoiding the difficulties of working with multiphase chemical reactions where the thermodynamic and kinetic constants are not well-defined.

2. Modeling

The Gibbs energy minimization problem is treated as an optimization problem, with the objective being to minimize the total Gibbs energy of a system that can contain CH_4 , CO_2 , CO , H_2 , H_2O and solid carbon, subject to atomic species conservation constraints. The pressure and temperature are fixed, as it is assumed that the reaction takes place in a heated reactor.

2.1. Objective function

In a given multicomponent system, the total Gibbs energy is given by:

$$G^T = \sum_{i=1}^N n_i \left(\Delta G_{fi}^0 + RT \ln \frac{\bar{f}_i}{f_i^0} \right) \quad (1)$$

With the chemical potential, μ_i , defined as:

$$\mu_i = \Delta G_{fi}^0 + RT \ln \frac{\bar{f}_i}{f_i^0} \quad (2)$$

$$G^T = \sum_{i=1}^N n_i \mu_i \quad (3)$$

The partial fugacity and standard state fugacities for every component is given respectively by:

$$\bar{f}_i = y_i \phi_i P \quad (4)$$

and $f_i^0 = P_0 = 0.1$ MPa.

The fugacity coefficient Φ_i can be obtained from the equation of state modeling the gas phase [29,41].

Solid carbon is expected to form during the reaction, and its Gibbs energy (kJ/mol) is given by:

$$G_C = n_C (\Delta G_{f_{Graphite}} + \Delta G_C^{dev}) \quad (5)$$

With $\Delta G_C^{dev} = 2.6 + 93/d$ being the particle-size dependent deviation parameter.

The total Gibbs energy of the reactive system is then the sum of the gas and solid phase Gibbs energies, assuming that the solid phase is only pure carbon:

$$G^T = \sum_{i=1}^{N-1} n_i \left(\Delta G_{f_i}^0 + RT \ln \frac{f_i}{f_i^0} \right) + n_C (\Delta G_{f_{Graphite}} + \Delta G_C^{dev}) \quad (6)$$

2.2. Constraints

The reactive system is assumed to contain only 6 potential compounds: CH₄, CO₂, CO, H₂, H₂O and solid carbon. Thus we define $n_f = [n_{CH_4} \ n_{CO_2} \ n_{H_2} \ n_{H_2O} \ n_C]$ as the vector containing the number of moles of each of the species at equilibrium, and n_0 is the vector containing the initial number of moles of each species.

We define matrix a such that a_{ij} is the number of moles of element i in a mole of species j . Matrix a is a 3×6 matrix with rows representing C, H, and O respectively, and columns representing the species in vector n respectively, then

$$a = \begin{bmatrix} 1 & 1 & 10 & 0 & 1 \\ 4 & 0 & 02 & 2 & 0 \\ 0 & 2 & 10 & 1 & 0 \end{bmatrix}$$

Let b be a 3×1 vector containing the initial number of moles of each atomic species, then

$$b = a \cdot n'_0 \quad (7)$$

The atomic conservation of atomic species then dictates: $a \cdot n'_f = b$.

Molar compositions should also be non-negative, and hence the problem statement becomes:

$$\min G^T = \sum_{i=1}^{N-1} n_i \left(\Delta G_{f_i}^0 + RT \ln \frac{f_i}{f_i^0} \right) + n_C \left(\Delta G_{f_{Graphite}} + 2.6 + \frac{93}{d} \right) \quad (8)$$

Subject to $a \times n'_f = b$.

where $n_0, n_f, d \geq 0$.

This problem was solved in MATLAB using fmincon with the interior-point algorithm for temperatures between 700 and 1000 °C and pressures between 1 and 20 bars for various catalyst diameters. The temperature range was chosen based on the review of a large number of experimental and theoretical studies [42–47] on dry reforming of methane, where the most relevant temperature range was identified. Although reforming reactions are favored at lower pressures due to the increase in the total number of moles in the system through the reaction, it was chosen to model up to 20 bars for the same reasons for which steam reformers and autothermal reformers are operated at high pressures; a higher syngas throughput is obtained through higher pressures and therefore it is of interest to predict the performance of the reactor at these conditions. Catalyst particle diameters considered are in the range of 5–20 nm, as these values give a reasonable representation of sintering throughout the catalyst lifetime [17]. Although nickel particle sizes can go up to ~100 nm, the results discussed here are limited to the range of 5–20 nm, since they sufficiently highlight the trends observable. Furthermore, the model by Alstrup [38] for the deviation from graphite thermodynamics does not assume a unique particle size or a very narrow particle size distribution, but rather correlates the deviation to the diameter of the largest particle catalyzing carbon growth. Still, it is assumed that as a catalyst sinters, the particle size distribution changes and the upper bound on catalyst particle size increases.

3. Results

Parameters studied are the methane and CO₂ conversion, defined as

$$X_i = \frac{n_{i,0} - n_{i,f}}{n_{i,0}} \times 100 \quad (9)$$

in addition to the H₂/CO ratio and the carbon formation, expressed as a molar percentage.

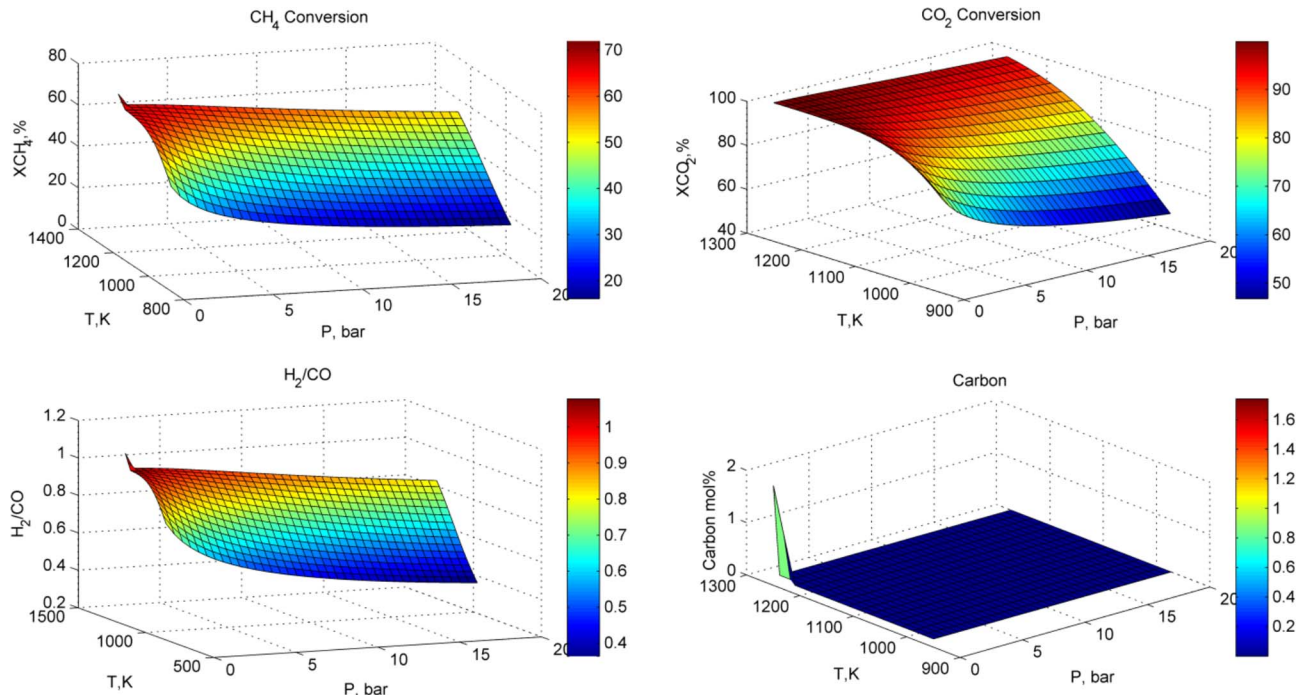


Fig. 1. Conversions, H₂/CO and solid carbon percentage as function of temperature and pressure for $d = 5$ nm and molar CH₄/CO₂ = 1.5.

$$C_s = \frac{n_{C,f}}{\sum_N n_{i,f}} \times 100 \quad (10)$$

The carbon limits are defined here as conditions of temperature and pressure where carbon deposition exceeds 0.1%. The initial molar composition of the reactive system is taken as 60% methane and 40% CO₂, as these values are an approximate representation of biogas composition. One must note that raw biogas also contains other gases such as H₂S, ammonia and water. The effect of these gases on the catalyst cannot be neglected, especially for hydrogen sulfide as they cause catalyst deactivation [48]. The deactivated catalyst then fails to make the reactive system reach equilibrium, and hence removal of these pollutants is usually done before introduction of the raw material to the reforming reactor, even when using methane as a feedstock for reforming. We can then safely assume negligible levels of contaminants in the system. Furthermore, the modeling of these compounds in a Gibbs Free energy minimization study is not representative since it cannot account for their effect on the catalyst directly.

3.1. Methane conversion

Figs. 1–3, 5 and 6 show the results of the simulation in terms of methane and CO₂ conversions, H₂/CO ratio and carbon formation as function of temperature and pressure. As is the case for an endothermic reaction, methane conversion increases with temperature, with a decreasing slope at higher temperatures, where the conversion reaches its maximum around 1000 °C and 1 bar. Lower pressures and high temperatures both favor the dry reforming reaction, as demonstrated by the increase in methane conversion with a decrease in pressure. A sharper increase in conversion is noticed at high temperature/low pressure, especially at low catalyst particle size. This jump is observed around the same P-T conditions at which the carbon limits are crossed, and therefore, the conversion spike is associated with the methane decomposition reaction producing solid carbon. Fig. 4 shows the evolution of methane and CO₂ conversion at 1000 °C and 1 bar in function of the catalyst particle diameter. A positive relationship is noticed, which can be related to the methane decomposition reaction proceeding further as the catalyst particle grows. This observation is in agreement with the results obtained for carbon formation, where the amount of carbon

formed at these conditions increases with particle size.

It is to note that the trend exhibited by methane conversion is in good agreement with other theoretical studies [11], although the conversion is lower. With CO₂ being the limiting reactant, it can be easily shown that the maximum conversion that can be attained by methane through the dry reforming reaction alone is 66.7% for a 60/40 methane/CO₂ initial composition, meaning that the reaction reaches almost complete conversion above ~850 °C and below ~8 bar. Methane conversions exceeding the theoretical maximum of 66.7% are attributed to carbon formation.

The obtained model shows a good agreement with experimental measurements of methane conversion on a Ni/Al₂O₃ catalyst with a nickel particle diameter of 23 nm at atmospheric pressure and CH₄/CO₂ molar ratio of 0.5 (experimental conditions by Ocsachoque et al. [49]), as shown in Fig. 7, and other nickel catalysts of varying diameters (Fig. 8). The model slightly overestimates experimental data, which is expected due to transport and kinetic limitations in experimental catalytic tests.

3.2. CO₂ conversion

The conversion of CO₂ is generally higher than that of methane, especially at lower temperatures. Carbon dioxide being the limiting reactant explains the higher conversion, although this trend has been noticed experimentally [42,50,51] and has been associated to the reverse water-gas shift reaction proceeding further at lower temperatures [52]. The CO₂ conversion is very weakly affected by the catalyst particle diameter, and is maximized at low pressures and high temperatures, and conversions above 99% can be reached above 1200 K.

No spike in conversion is observed in CO₂ when the carbon limits are crossed, unlike in methane, meaning that methane dissociation is the main source of carbon formation at a CH₄/CO₂ ratio of 1.5. However, it is reported [53] that CO disproportionation is the main contributor to carbon deposition. The difference between the present work and the literature is probably due to CO₂ reaching a conversion close to 100% even outside the carbon limits.

Simulation results for an equimolar feed of methane and carbon dioxide (Fig. 3) show that CO₂ conversion does not increase in a sharper

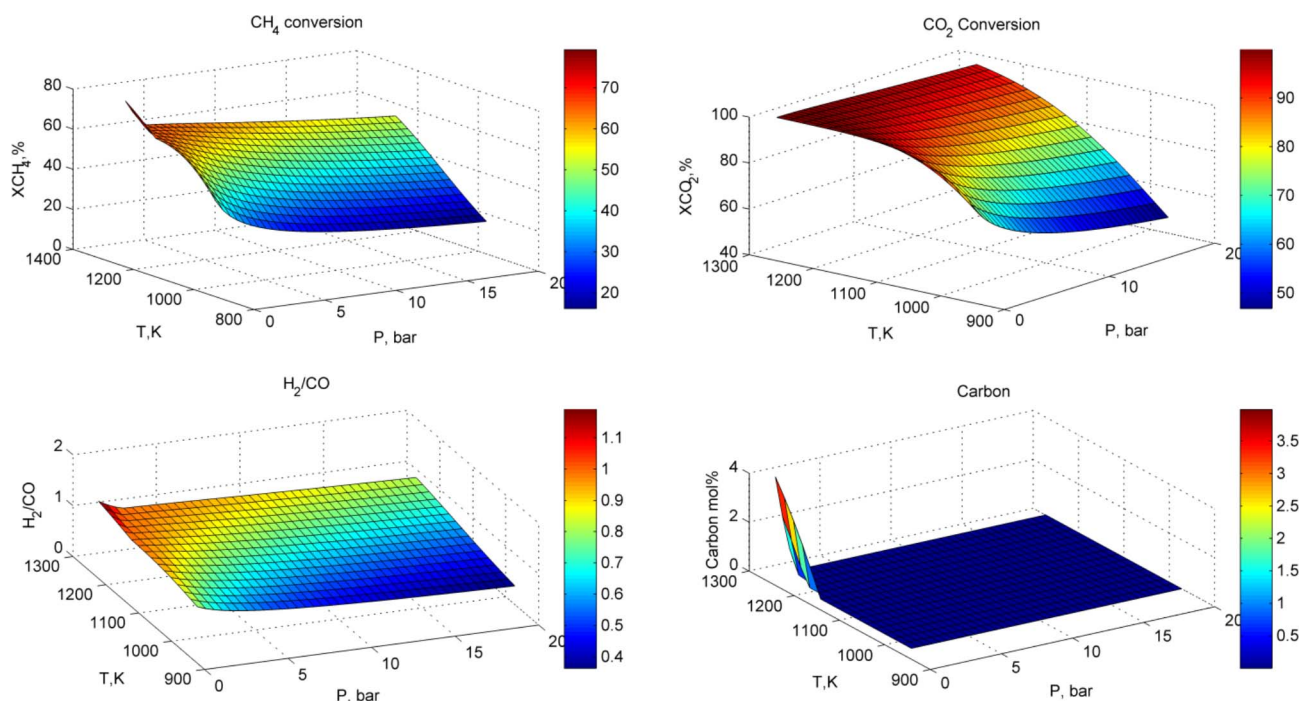


Fig. 2. Conversions, H₂/CO and solid carbon percentage as function of temperature and pressure for $d = 7$ nm and molar CH₄/CO₂ = 1.5.

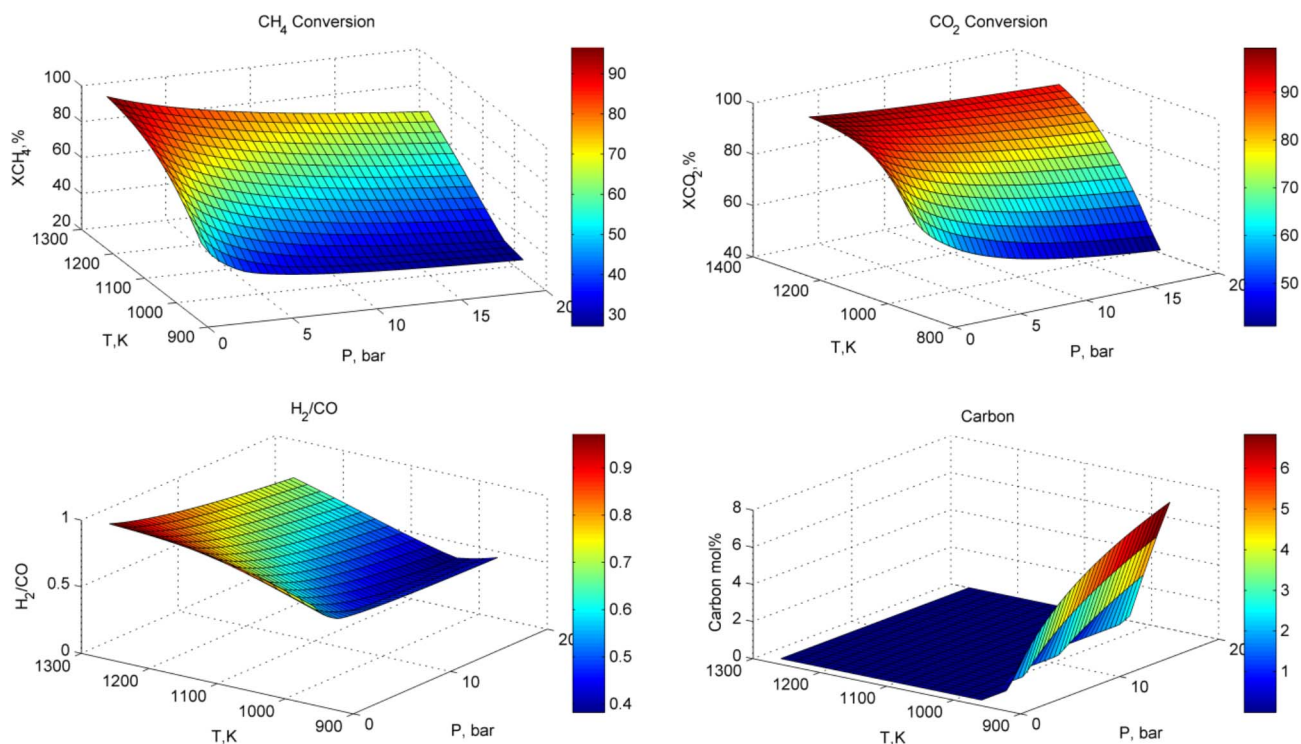


Fig. 3. Conversions, H₂/CO and solid carbon percentage as function of temperature and pressure for d = 15 nm and molar CH₄/CO₂ = 1.0.

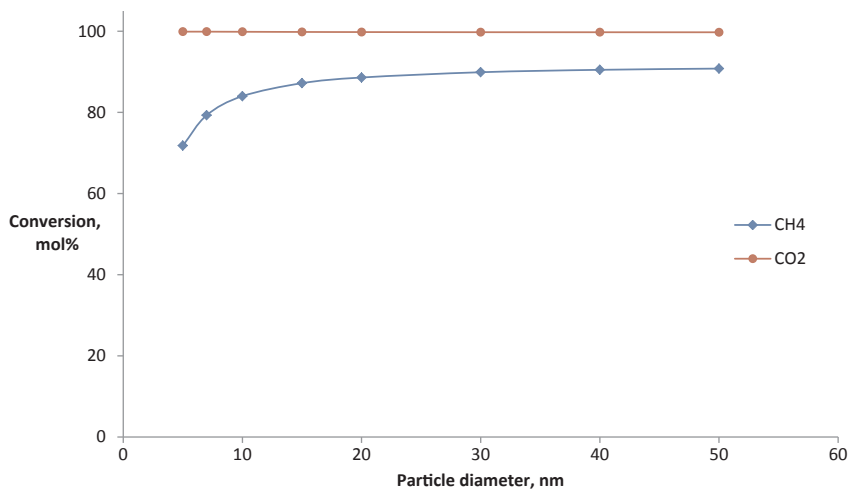


Fig. 4. Methane and CO₂ conversions at 1000 °C and 1 bar as a function of particle diameter for molar CH₄/CO₂ ratio of 1.5.

fashion at high temperatures. The methane spike is not observed, but no carbon is formed at higher temperatures, in perfect accordance with Bradford and Vannice [53]. However, at lower temperatures, carbon deposition is increased as compared to the 60/40 methane/CO₂ system where carbon dioxide is depleted essentially through the dry reforming reaction. Trends in methane and carbon dioxide conversion obtained are in good agreement with the literature [54] and experimental measurements (Figs. 7 and 8).

3.3. H₂/CO ratio

Average H₂/CO ratio is slightly below unity for all catalyst particle sizes, with a convex relationship with respect to pressure that is less noticeable at smaller particle sizes. The minimum is reached at lower temperatures and moderate to high pressures (10–20 bars) while the maximum is generally reached at lower pressures and high temperatures. This pattern is explained by the mutual effect of the reverse

water-gas shift reaction and the two main modes of carbon formation, through CH₄ or CO decomposition, reaching different extents at different conditions. At lower temperatures, the exothermic Boudouard reaction is favored over the methane decomposition reaction. Furthermore, the reverse water-gas shift reaction converts hydrogen into water, causing a decrease in the H₂/CO ratio. At higher temperatures, the reverse water-gas shift reaction is less favored, hence the increase in H₂ presence. Methane decomposition into carbon and hydrogen also causes the H₂/CO ratio to rise above unity at conditions of low pressure and high temperature. At catalyst diameters larger than 15 nm, the hydrogen/CO ratio becomes convex with respect to temperature as well. This trend can be explained by the effect of the exothermic Boudouard reaction yielding less carbon as temperature increases while the endothermic methane decomposition reaction only forms carbon at high temperatures. The behavior of the hydrogen/CO ratio is in agreement with Atashi et al. [29] except for temperatures above 1200 K where a drop in the H₂/CO ratio was reported while in

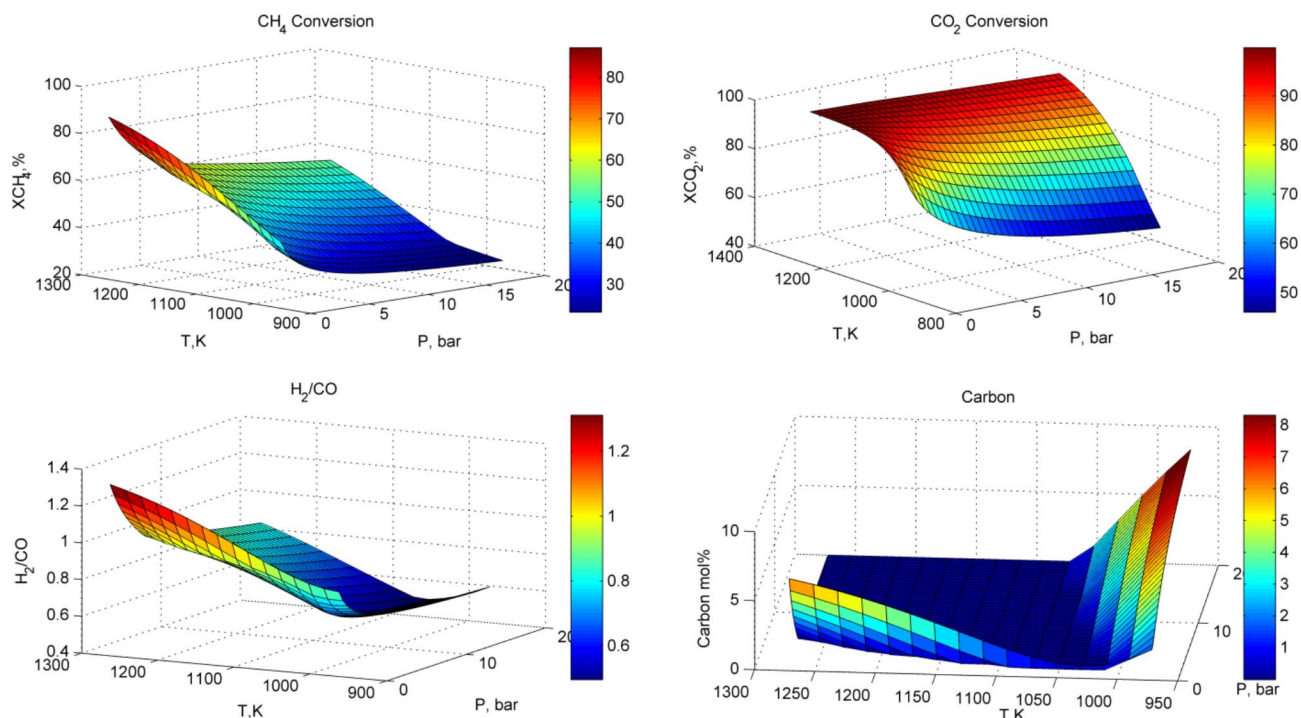


Fig. 5. Conversions, H_2/CO and solid carbon percentage as function of temperature and pressure for $d = 15$ nm and molar $CH_4/CO_2 = 1.5$.

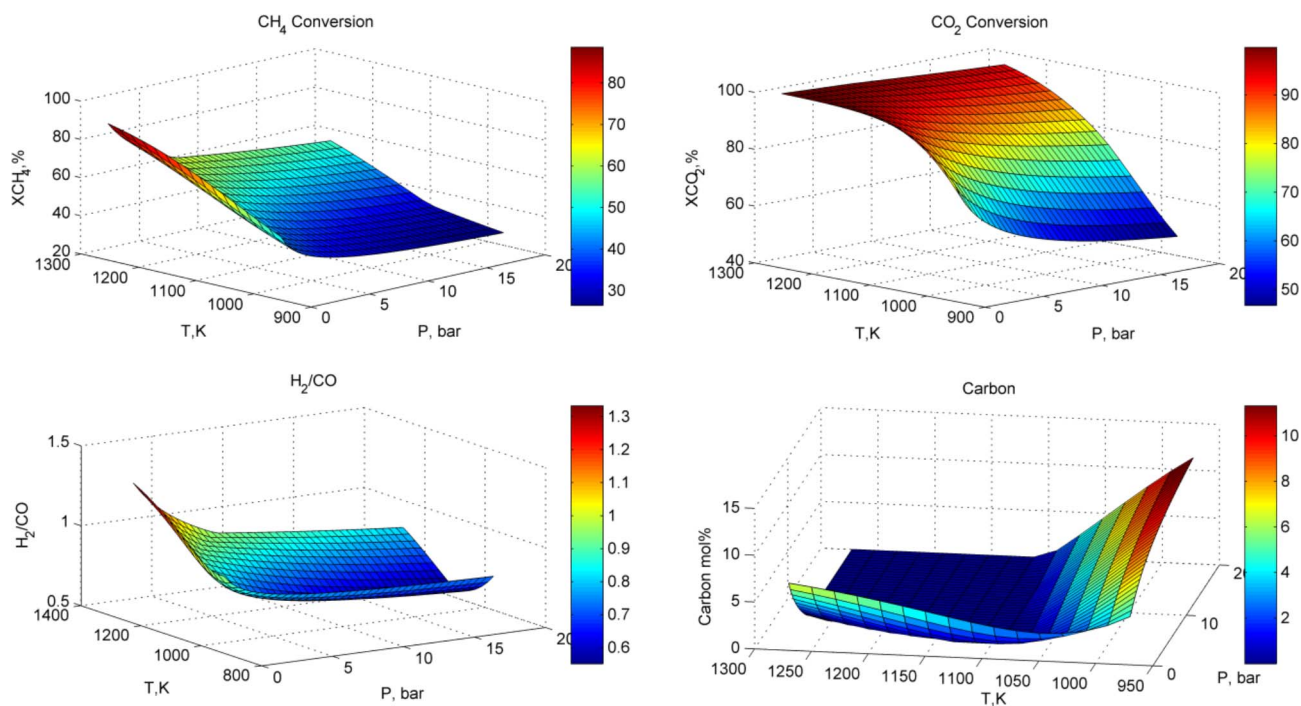


Fig. 6. Conversions, H_2/CO and solid carbon percentage as function of temperature and pressure for $d = 20$ nm and molar $CH_4/CO_2 = 1.5$.

this work a monotonous trend was obtained.

3.4. Carbon formation

The patterns of carbon deposition noticed correspond exactly to theoretical predictions: the amount of carbon formed increases with catalyst particle size, especially above 6 nm which is the thermodynamic stability limit for carbon deposits on the catalyst, corresponding to the critical diameter of 80 atoms described by Bengaard [19] and confirmed by Kim et al. [51]. Table 1 shows this pattern

corresponds to experimental results obtained by different groups. The behavior of carbon formation is observed to be similar to simulation results by Tsai and Wang [56] but carbon mole fractions calculated are lower: carbon formation for an equimolar CH_4/CO_2 feed was found to reach a maximum of 7–8 mol% while the mole fractions obtained by [56] went as high as 20 mol%.

Carbon seems to form in two different modes: at low pressures and high temperatures, moderate amounts are formed especially on fine catalysts. Under these conditions, the main contributor to carbon deposition is methane, as its decomposition into hydrogen is endothermic

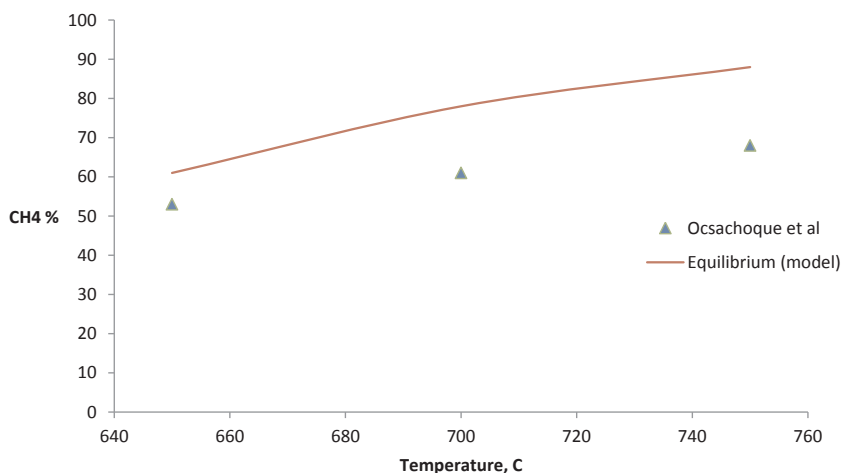


Fig. 7. Comparison of simulation results with experimental measurements from [49] with $d = 23$ nm and molar $\text{CH}_4/\text{CO}_2 = 0.5$ at $P = 1$ bar.

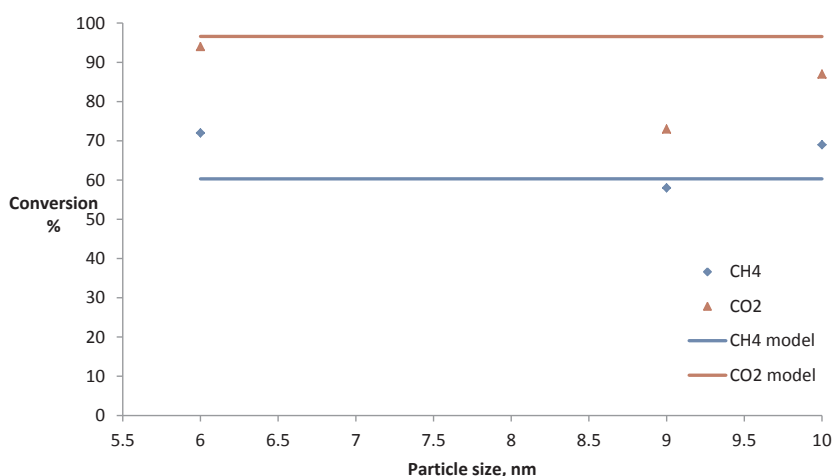


Fig. 8. Comparison of model with experimental data from [55] for $T = 800$ °C, 1 atm and $\text{CH}_4/\text{CO}_2 = 1.5$.

and increases the total number of moles, hence the low pressure requirement. Furthermore, at $d = 15$ nm, carbon forms at these conditions for $\text{CH}_4/\text{CO}_2 = 1.5$ but not for an equimolar system. In other words, the presence of methane is correlated to the formation of carbon at the conditions that favor methane decomposition. At low temperatures, solid carbon only forms at higher pressures, and the amount formed decreases with increasing temperature but is larger than high temperature coke. This trend is typical of CO as a precursor to carbon formation by the Boudouard reaction, as it is exothermic and decreases the total number of moles of gas, therefore requiring higher pressures from Le Chatelier's principle. It can also be noticed that an increase in CO_2 concentration from 40% to 50% in the initial system causes an increase in the amount of carbon formed at low temperatures. Although the expected result is the reverse Boudouard reaction to be favored, the added CO_2 forms extra CO that reacts to give solid carbon. Fig. 9 shows the carbon limits beyond which solid carbon forms more than 0.1 mol% of the system. As the diameter of the metallic catalyst particle increases, carbon is expected to form in a wider region of temperature and

pressure. At $d = 15$ nm, the two distinct regions of carbon presence overlap and carbon is then expected at high temperatures or high pressures.

The positive relationship between pressure and carbon formation is in agreement with the literature but this study noted that an increase in the CO_2 content of the initial system caused an increase in solid carbon at low pressures while Sun et al. [54] found the opposite trend.

The optimal operating conditions should guarantee a high conversion while remaining outside the carbon limits and maintaining a H_2/CO ratio close to unity. Conditions of both high temperatures and pressures (1200 K, 10–15 bar) are not expected to yield carbon, but the methane conversion is not maximized and hydrogen/CO ratio is around 0.8. Equimolar H_2 and CO are obtained at approximately 1100–1200 K and 5–10 bar with satisfactory CH_4 and CO_2 conversion, but the risk of carbon formation is high since the carbon limits are close. From an industrial point of view, a fresh catalyst with high dispersion can tolerate such an operation but the catalyst has to be carefully monitored and replaced when the upper limit on particle size is around 10 nm.

Table 1
Experimental results for various nickel catalysts.

Catalyst	Catalyst size (nm)	T (°C)	CH_4 (mol%)	CO_2 (mol%)	Carbon	Reference
8% Ni/ Al_2O_3	14	860	71.5	96	0.18 g/gcat (300 min)	[9]
8% Ni/20Ce- Al_2O_3	10	860	70.6	97.1	0.168 g/gcat (300 min)	[9]
8%Ni/ Al_2O_3 edf	6	800	72	94	0.96 wt%	[55]
8%Ni/ Al_2O_3 wet	10	800	69	87	6.17 wt%	[55]
8%Ni/ Al_2O_3 iwi	9	800	58	73	3.04 wt%	[55]

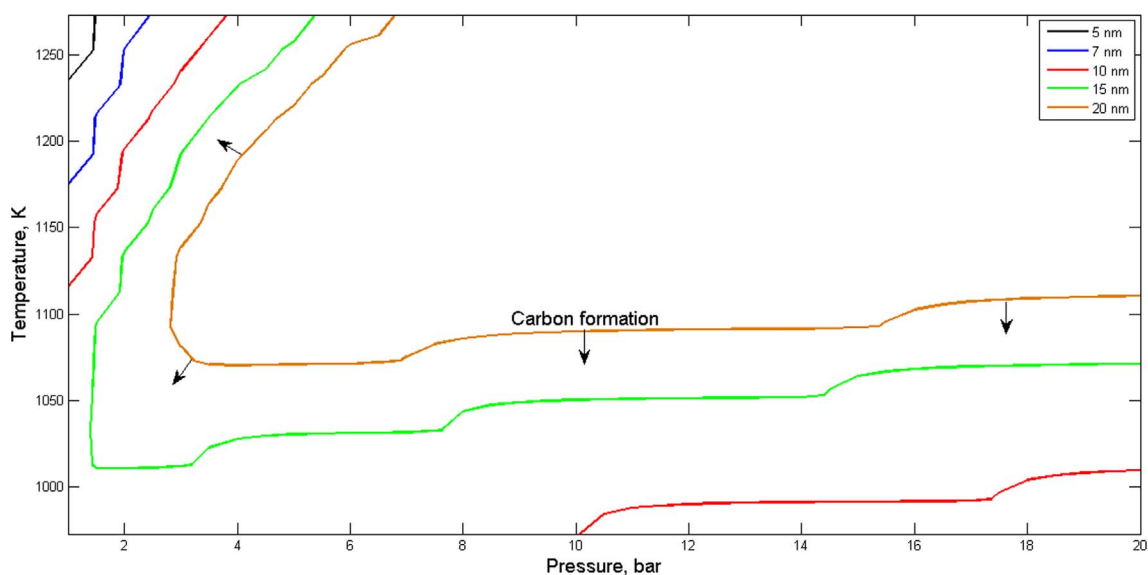


Fig. 9. Carbon limits for $\text{CH}_4/\text{CO}_2 = 1.5$ as a function of catalyst particle size.

This study further highlights the requirement of having a stable catalyst that can resist sintering for long periods of time. From the catalyst designer's perspective, this means that the catalyst should have a very strong active metal-support interaction (spinel structure), which in turn renders the catalyst more difficult to reduce at process startup, requiring higher temperatures and longer reduction times. The corrosive reducing environment and higher temperatures significantly reduce the reactor service life, which in turn increases the maintenance costs of the plant. An optimization study should then be performed to find the best balance between catalyst cost and maintenance cost of the reformer.

4. Conclusion

The formation of carbon was found to be a dynamic phenomenon that is not only a function of temperature and pressure but also of the catalyst, with larger active metal particles yielding carbon at more moderate conditions. Though the impact of the catalyst on carbon formation has been demonstrated by countless experimental studies, this work offers a theoretical tool that accounts for the effect of sintering on reactor performance. Optimal process conditions were found to be dangerously close to the carbon limits, hence highlighting the need for a fine catalyst particle size, ideally below 5 nm, to avoid excessive carbon deposition. Conditions of very high temperature and low pressures were found to yield moderate amounts of carbon mainly through methane decomposition, while conditions of low temperature and high pressure gave higher amounts of carbon through the Boudouard reaction.

References

- Muneer T, Asif M, Kubie J. Generation and transmission prospects for solar electricity: UK and global markets. *Energy Convers Manage* 2003;44:35–52.
- Li X. Diversification and localization of energy systems for sustainable development and energy security. *Energy Policy* 2005;33:2237–43.
- Usman M, Wan Daud WMA, Abbas HF. Dry reforming of methane: influence of process parameters—a review. *Renew Sustain Energy Rev* 2015;45:710–44.
- Noor ZZ, Yusuf RO, Abba AH, Abu Hassan MA, Mohd Din MF. An overview for energy recovery from municipal solid wastes (MSW) in Malaysia scenario. *Renew Sustain Energy Rev* 2013;20:378–84.
- Massoud M, Merehbi F. Guide to municipal solid waste management. American University of Beirut-Nature Conservation Center; 2016.
- Farshchi Tabrizi F, Mousavi SAHS, Atashi H. Thermodynamic analysis of steam reforming of methane with statistical approaches. *Energy Convers Manage* 2015;103:1065–77.
- Cau G, Cocco D, Petrollese M, Knudsen Kær S, Milan C. Energy management strategy based on short-term generation scheduling for a renewable microgrid using a hydrogen storage system. *Energy Convers Manage* 2014;87:820–31.
- Rostrup-Nielsen JR. Production of synthesis gas. *Catal Today* 1993;18:305–24.
- Bereketidou OA, Goula MA. Biogas reforming for syngas production over nickel supported on ceria–alumina catalysts. *Catal Today* 2012;195:93–100.
- Hu YH, Ruckenstein E. Catalytic conversion of methane to synthesis gas by partial oxidation and CO_2 reforming. *Adv Catal* 2004;48:297–345.
- Nikoo MK, Amin NAS. Thermodynamic analysis of carbon dioxide reforming of methane in view of solid carbon formation. *Fuel Process Technol* 2011;92:678–91.
- Navarro RM, Álvarez-Galván MC, Rosa F, Fierro JLG. Hydrogen production by oxidative reforming of hexadecane over Ni and Pt catalysts supported on Ce/La-doped Al_2O_3 . *Appl Catal A* 2006;297:60–72.
- Lavoie J-M. Review on dry reforming of methane, a potentially more environmentally-friendly approach to the increasing natural gas exploitation. *Front Chem* 2014;2.
- Ginsburg JM, Piña J, El Solh T, de Lasa HI. Coke formation over a nickel catalyst under methane dry reforming conditions: thermodynamic and kinetic models. *Ind Eng Chem Res* 2005;44:4846–54.
- Bradford MCJ, Vannice MA. Catalytic reforming of methane with carbon dioxide over nickel catalysts II. Reaction kinetics. *Appl Catal A: Gener* 1996;142:97–122.
- Pakhare D, Spivey J. A review of dry (CO_2) reforming of methane over noble metal catalysts. *Chem Soc Rev* 2014;43:7813–37.
- Sehested J. Four challenges for nickel steam-reforming catalysts. *Catal Today* 2006;111:103–10.
- Chen RY, Chen YC, Yu CT, Chung JN. Thermodynamic analysis of dry reforming of CH_4 with CO_2 at high pressures. *J Nat Gas Sci Eng* 2015;26:617–29.
- Bengard HS, Nørskov JK, Sehested J, Clausen BS, Nielsen LP, Molenbroek AM, et al. Steam reforming and graphite formation on Ni catalysts. *J Catal* 2002;209:365–84.
- Khani Y, Shariatinia Z, Bahadoran F. High catalytic activity and stability of ZnLaAlO_4 supported Ni, Pt and Ru nanocatalysts applied in the dry, steam and combined dry-steam reforming of methane. *Chem Eng J* 2016;299:353–66.
- Hou Z, Chen P, Fang H, Zheng X, Yashima T. Production of synthesis gas via methane reforming with CO_2 on noble metals and small amount of noble-(Rh-) promoted Ni catalysts. *Int J Hydrogen Energy* 2006;31:555–61.
- Simakov DSA, Wright MM, Ahmed S, Mokheimer EMA, Román-Leshkov Y. Solar thermal catalytic reforming of natural gas: a review on chemistry, catalysis and system design. *Catal Sci Technol* 2015;5:1991–2016.
- Annesini MC, Piemonte V, Turchetti L. Carbon formation in the steam reforming process: a thermodynamic analysis based on the elemental compositions. *Chem Eng Trans* 2007;11:21–6.
- de Souza TL, Rossi CdCRdS, Alonso CG, Guirardello R, Cabral VF, Fernandes-Machado NRC, et al. Thermodynamic analysis of autothermal reforming of methane via entropy maximization: hydrogen production. *Int J Hydrogen Energy* 2014;39:8257–70.
- Solsvik J, Haug-Warberg T, Jakobsen HA. Implementation of chemical reaction equilibrium by Gibbs and Helmholtz energies in tubular reactor models: application to the steam–methane reforming process. *Chem Eng Sci* 2016;140:261–78.
- Li Y, Wang Y, Zhang X, Mi Z. Thermodynamic analysis of autothermal steam and CO_2 reforming of methane. *Int J Hydrogen Energy* 2008;33:2507–14.
- Amin NAS, Yaw TC. Thermodynamic equilibrium analysis of combined carbon dioxide reforming with partial oxidation of methane to syngas. *Int J Hydrogen Energy* 2007;32:1789–98.
- Challiwala MS, Ghouri MM, Linke P, El-Halwagi MM, Elbasher NO. A combined thermo-kinetic analysis of various methane reforming technologies: comparison with dry reforming. *J CO₂ Util* 2017;17:99–111.
- Atashi H, Gholizadeh J, Farshchi Tabrizi F, Tayebi J, Seyyed Mousavi SAH.

- Thermodynamic analysis of carbon dioxide reforming of methane to syngas with statistical methods. *Int J Hydrogen Energy*; 2016.
- [30] Jafarbegloo M, Tarlani A, Mesbah AW, Sahebdehfar S. Thermodynamic analysis of carbon dioxide reforming of methane and its practical relevance. *Int J Hydrogen Energy* 2015;40:2445–51.
- [31] Noureldin MMB, Elbashir NO, El-Halwagi MM. Optimization and selection of reforming approaches for syngas generation from natural/shale gas. *Ind Eng Chem Res* 2014;53:1841–55.
- [32] Ayodele BV, Cheng CK. Process modelling, thermodynamic analysis and optimization of dry reforming, partial oxidation and auto-thermal methane reforming for hydrogen and syngas production. *Chem Prod Process Model* 2015;10.
- [33] Nematollahi B, Rezaei M, Lay EN, Khajenoori M. Thermodynamic analysis of combined reforming process using Gibbs energy minimization method: in view of solid carbon formation. *J Nat Gas Chem* 2012;21:694–702.
- [34] Papadopoulou C, Matalis H, Verykios X. Utilization of biogas as a renewable carbon source: dry reforming of methane; 2012.
- [35] Rostrup-Nielsen JR, Sehested J, Norskov JK. Hydrogen and synthesis gas by steam- and CO₂ reforming. *Adv Catal* 2002;47:65–139.
- [36] Dent FJ, Moignard LA, Eastwood AH, Blackburn WH, Hebden D. An investigation into the catalytic synthesis of methane for town gas manufacture. *Trans: Inst Gas Eng* 1945–1946;95:602–704.
- [37] Alstrup I, Tavares MT, Bernardo CA, Sorensen O, Rostrup-Nielsen JR. Carbon formation on nickel and nickel-copper alloy catalysts. *Mater Corros* 1998;49:367–72.
- [38] Alstrup I. A new model explaining carbon filament growth on nickel, iron, and Ni-Cu alloy catalysts. *J Catal* 1988;109:241–51.
- [39] Rostrup-Nielsen J. Equilibria of decomposition reactions of carbon monoxide over nickel catalysts. *J Catal* 1972;27:343–56.
- [40] Kalai DY. Dry reforming of methane: catalyst development and thermodynamic analysis. Faculty of Science and Technology, University of Stavanger; 2015.
- [41] Smith HCVNJM, Abbott MM. Introduction to chemical engineering thermodynamics. 7th ed. New York: Mc Graw-Hill Book Company; 2005.
- [42] Xu J, Zhou W, Li Z, Wang J, Ma J. Biogas reforming for hydrogen production over nickel and cobalt bimetallic catalysts. *Int J Hydrogen Energy* 2009;34:6646–54.
- [43] Liu D, Quek XY, Cheo WNE, Lau R, Borgna A, Yang Y. MCM-41 supported nickel-based bimetallic catalysts with superior stability during carbon dioxide reforming of methane: Effect of strong metal-support interaction. *J Catal* 2009;266:380–90.
- [44] Xiancai L, Min W, Zhihua L, Fei H. Studies on nickel-based catalysts for carbon dioxide reforming of methane. *Appl Catal A* 2005;290:81–6.
- [45] Arbag H, Yasyerli S, Yasyerli N, Dogu G. Activity and stability enhancement of Ni-MCM-41 catalysts by Rh incorporation for hydrogen from dry reforming of methane. *Int J Hydrogen Energy* 2010;35:2296–304.
- [46] Barroso-Quiroga MM, Castro-Luna AE. Catalytic activity and effect of modifiers on Ni-based catalysts for the dry reforming of methane. *Int J Hydrogen Energy* 2010;35:6052–6.
- [47] Wu T, Cai W, Zhang P, Song X, Gao L. Cu-Ni@SiO₂ alloy nanocomposites for methane dry reforming catalysis. *RSC Adv* 2013;3:23976.
- [48] Jablonski WS, Villano SM, Dean AM. A comparison of H₂S, SO₂, and COS poisoning on Ni/YSZ and Ni/K₂O-CaAl₂O₄ during methane steam and dry reforming. *Appl Catal A* 2015;502:399–409.
- [49] Ocsachoque M, Pompeo F, Gonzalez G. Rh-Ni/CeO₂-Al₂O₃ catalysts for methane dry reforming. *Catal Today* 2011;172:226–31.
- [50] Lucrédio AF, Assaf JM, Assaf EM. Reforming of a model biogas on Ni and Rh-Ni catalysts: effect of adding La. *Fuel Process Technol* 2012;102:124–31.
- [51] Kim J-H, Suh DJ, Park T-J, Kim K-L. Effect of metal particle size on coking during CO₂ reforming of CH₄ over Ni-alumina aerogel catalysts. *Appl Catal A* 2000;197:191–200.
- [52] Wang S, Lu GQ, Millar GJ. Carbon dioxide reforming of methane to produce synthesis gas over metal-supported catalysts: state of the art. *Energy Fuels* 1996;10:896–904.
- [53] Bradford MCJ, Vannice MA. CO₂ reforming of CH₄. *Catal Rev* 1999;41:1–42.
- [54] Sun Y, Ritchie T, Hla SS, McEvoy S, Stein W, Edwards JH. Thermodynamic analysis of mixed and dry reforming of methane for solar thermal applications. *J Nat Gas Chem* 2011;20:568–76.
- [55] Goula MA, Charisiou ND, Papageridis KN, Delimitis A, Pachatouridou E, Iliopoulou EF. Nickel on alumina catalysts for the production of hydrogen rich mixtures via the biogas dry reforming reaction: influence of the synthesis method. *Int J Hydrogen Energy* 2015;40:9183–200.
- [56] Tsai H-L, Wang C-S. Thermodynamic equilibrium prediction for natural gas dry reforming in thermal plasma reformer. *J Chin Inst Eng* 2008;31:891–6.